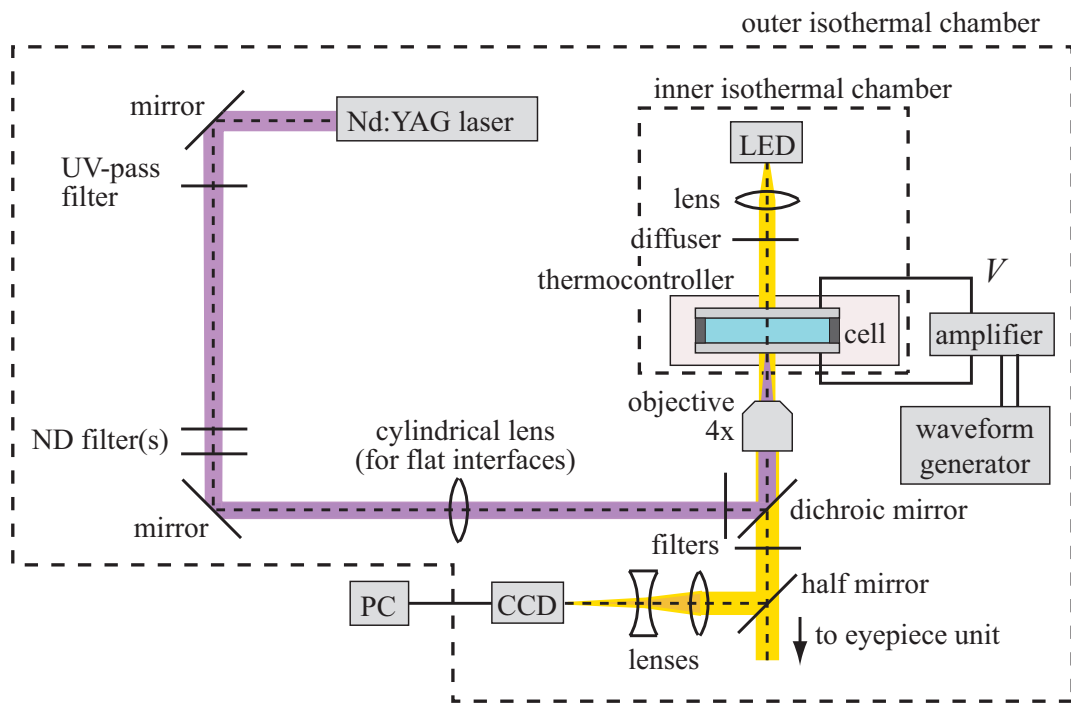


# Growing Interfaces Uncover Universal Fluctuations behind Scale Invariance

Kazumasa A. Takeuchi, Masaki Sano, Tomohiro Sasamoto & Herbert Spohn

Supplementary Information

## Supplementary Figure



**Supplementary Figure 1 | Schematic diagram of the experimental setup.** CCD: charge-coupled device camera, LED: light-emitting diode, ND: neutral density, PC: computer, UV: ultraviolet. The convection cell consists of two parallel glass plates with transparent electrodes (indium-tin oxide) and a polyester-film spacer of thickness  $12\ \mu\text{m}$ , which enclose a region of  $16\ \text{mm} \times 16\ \text{mm}$  for the convection. The inner surfaces are coated with *N,N*-dimethyl-*N*-octadecyl-3-aminopropyltrimethoxysilyl chloride in order to realise the homeotropic alignment of the liquid crystal. During the experiments, we keep a constant temperature of the cell at  $25\ ^\circ\text{C}$  with fluctuations about  $10^{-3}\ \text{K}$ , using two nested isothermal chambers (dashed lines) and a thermocontroller with a proportional-integral-derivative feedback loop (see Fig. 2b of our past publication<sup>21</sup> for details). The convection is observed through the transmitted light from a light-emitting diode and recorded by a CCD camera. A cylindrical lens is inserted for the flat-interface experiments, and the laser intensity is adjusted by ND filters on the optical path.

## Supplementary Notes

### 1. Parameter estimation

Here we explain how to estimate the values of the two parameters  $v_\infty$  and  $\Gamma$  in equation (2) of the paper:

$$h(t) \simeq v_\infty t + (\Gamma t)^{1/3} \chi. \quad (3)$$

The linear growth rate  $v_\infty$  is simply measured from the time derivative of the mean height, which reads

$$\frac{d\langle h \rangle}{dt} \simeq v_\infty + at^{-2/3} \quad (4)$$

with a coefficient  $a \approx \Gamma^{1/3}\langle \chi \rangle / 3$ . Our experimental data indeed show this linear relation between  $d\langle h \rangle / dt$  and  $t^{-2/3}$  (Supplementary Fig. 2ab). The linear regression then provides a precise estimate of  $v_\infty$  from its  $y$  intercept, at

$$v_\infty = \begin{cases} 33.24(4) \text{ } \mu\text{m/s} & (\text{circular}), \\ 32.75(3) \text{ } \mu\text{m/s} & (\text{flat}), \end{cases} \quad (5)$$

Here the numbers in the parentheses indicate the range of error in the last digit.

The amplitude  $\Gamma$  of the  $t^{1/3}$ -fluctuations is measured from the second order cumulant of the height

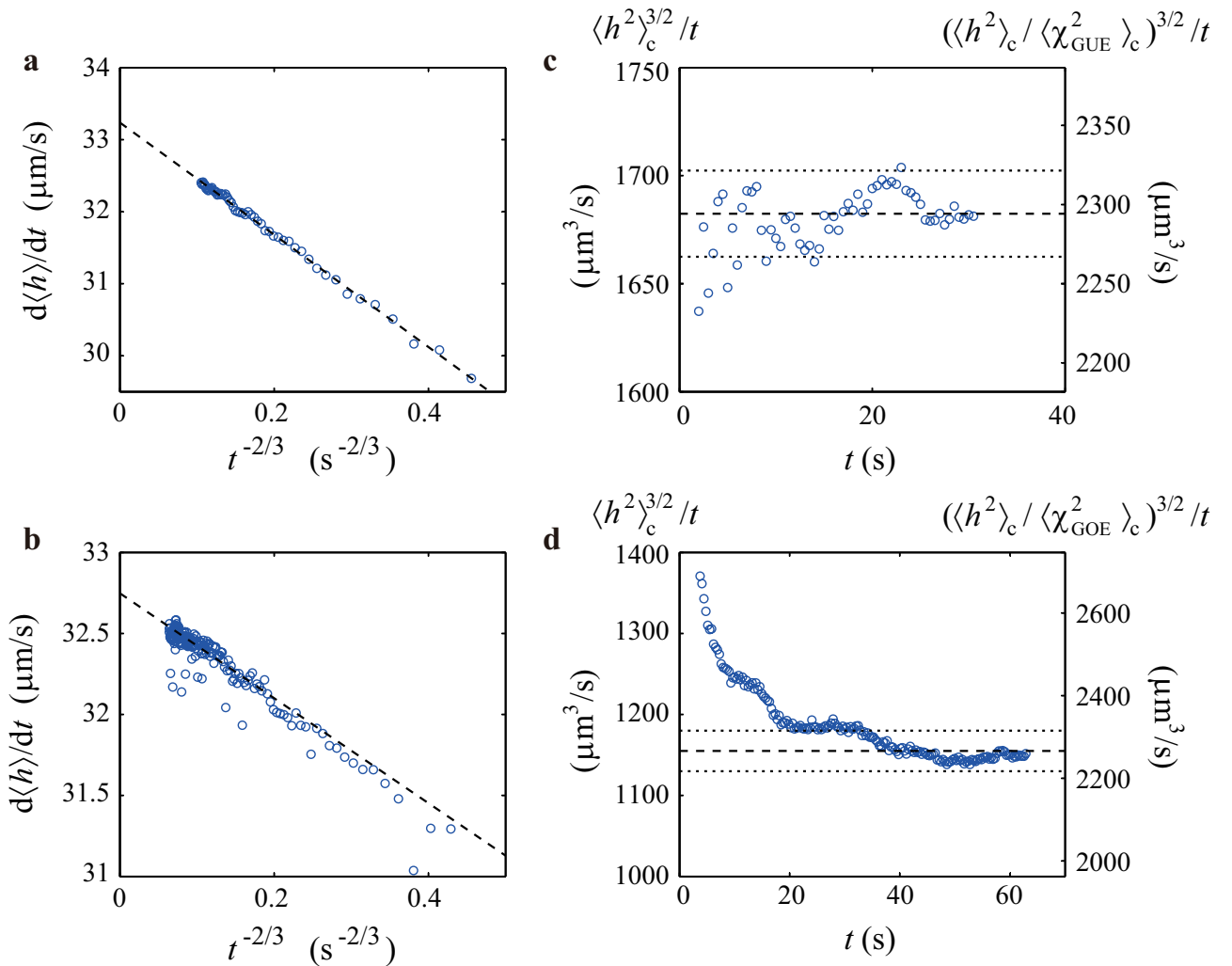
$$\langle h^2 \rangle_c = W(t)^2 \simeq (\Gamma t)^{2/3} \langle \chi^2 \rangle_c. \quad (6)$$

Its amplitude at late times determines the most probable value and the confidence interval of the parameter  $\Gamma$  (Supplementary Fig. 2cd). The actual value of  $\Gamma$  depends on how to normalise the variance  $\langle \chi^2 \rangle_c$ . In Supplementary Fig. 2cd we show values under two reasonable normalisations,  $\langle \chi^2 \rangle_c$  being 1 (left axes) or the variance of the expected TW distribution (right axes). We adopt in the paper the latter normalisation to allow direct comparison to the theoretical distribution functions in the literature, which gives

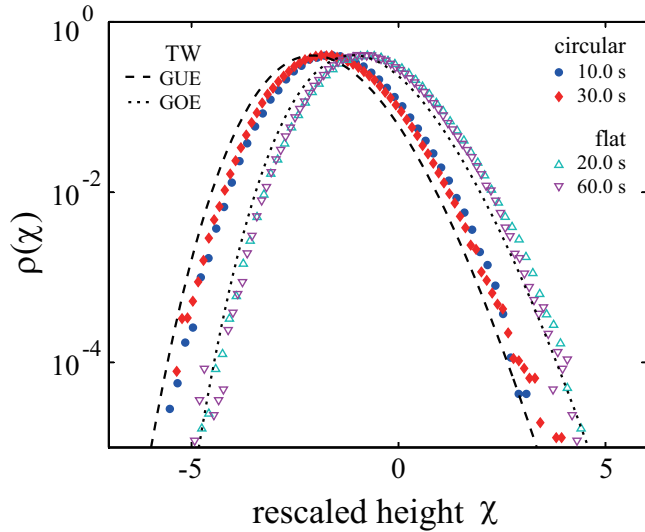
$$\Gamma = \begin{cases} 2.29(3) \times 10^3 \text{ } \mu\text{m}^3/\text{s} & (\text{circular}), \\ 2.27(5) \times 10^3 \text{ } \mu\text{m}^3/\text{s} & (\text{flat}), \end{cases} \quad (7)$$

but the same conclusion is reached with the former normalisation (Supplementary Fig. 3).

Note that, theoretically, the circular and flat interfaces should share the same parameter values. This also favors the choice of the normalisation with  $\langle \chi_{\text{GUE}}^2 \rangle_c$  and  $\langle \chi_{\text{GOE}}^2 \rangle_c$ . The slight difference in the estimates of  $v_\infty$  is most probably due to the aging of the liquid crystal sample, which is a well-known property of MBBA<sup>19,21</sup>, during the few days which separated the two series of the experiments. On the other hand, no measurable shift of the parameter values was detected during a single set of the experiments.



**Supplementary Figure 2 | Parameter estimation.** **a,b**, Estimation of the linear growth rate  $v_\infty$  for the circular (**a**) and flat (**b**) interfaces. The instantaneous growth speed  $d\langle h \rangle / dt$ , averaged over 2.5 s here, is plotted against  $t^{-2/3}$ . The linear regression (dashed line) provides a precise estimate of  $v_\infty$  from its  $y$  intercept. **c,d**, Estimation of the amplitude  $\Gamma$  of the  $t^{1/3}$ -fluctuations for the circular (**c**) and flat (**d**) interfaces. The amplitude of the second order cumulant  $\langle h^2 \rangle_c$  at late times determine the most probable value (dashed line) and the confidence interval (dotted lines) of the amplitude  $\Gamma$ . The left and right axes indicate the value of  $\Gamma$  under the normalisation  $\langle \chi^2 \rangle_c$  being 1 (left axes) and the variance of the expected TW distribution (right axes).



**Supplementary Figure 3 | Local height distribution.** The same data as in Fig. 2b is shown under the normalisation  $\langle \chi^2 \rangle_c = 1$ . We can still confirm that the circular and flat interfaces exhibit distinct distributions in agreement with the GUE and GOE TW distributions, respectively, with the finite-time effects evidenced in Fig. 2cd. The different normalisation does not affect the results of the finite-time effects, since it only multiplies the cumulants by constant factors.

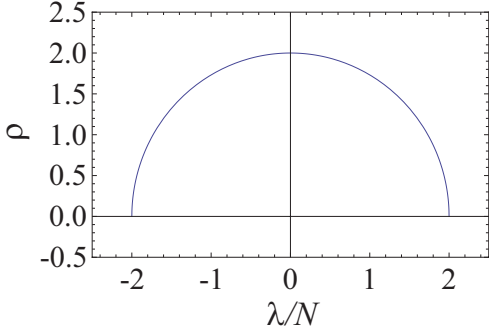
## 2. Random matrices and growth processes

Here we sketch how the probability densities in random matrix theory arise in the context of growth processes. On the basis of this relation we also illustrate how the curved and flat initial profiles lead to the different height statistics, as evidenced in our experiment.

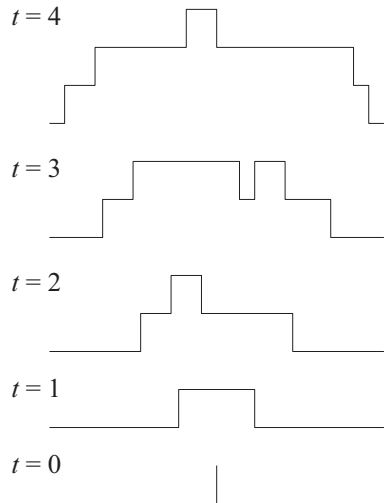
### 2.1. Random matrices

A random matrix is a matrix with random entries. Since Wigner found one of the earliest applications in the description of the energy levels of highly excited nuclei<sup>35</sup>, random matrices have turned out to be surprisingly useful in many areas of science, ranging from such pure mathematics as number theory to wireless communications and economics<sup>22,36,37</sup>.

A prominent example of random matrices is the Gaussian unitary ensemble (GUE), which is already mentioned in the main text. It comprises  $N \times N$  hermitian matrices  $A$  with the statistical weight  $Z_N^{-1} \exp(-\frac{1}{2N} \text{Tr } A^2)$ , where  $Z_N$  is the normalizing constant. In the studies of random matrices, one is often interested in statistical properties of their eigenvalues. The factor  $1/N$  in front of the trace is chosen so that typical distances between eigenvalues are of order 1. A well-known property of the eigenvalues is the semicircle law (Supplementary Fig. 4), which states that the average density of



**Supplementary Figure 4** | Semicircle law.



**Supplementary Figure 5** | Polynuclear growth (PNG) model.

GUE eigenvalues  $\lambda$  is given by  $\rho(\lambda/N)$  with

$$\rho(x) = \frac{1}{2\pi} \sqrt{4 - x^2} \text{ for } |x| \leq 2, \quad \rho(x) = 0 \text{ for } |x| \geq 2. \quad (8)$$

This implies that most eigenvalues of GUE lie in the region  $|\lambda| \leq 2N$ . In particular, the largest eigenvalue is close to  $2N$ .

For GUE, one can find an explicit expression for the joint probability density of the eigenvalues,  $\lambda_i$ ,  $1 \leq i \leq N$ , which reads

$$p(\lambda_1, \dots, \lambda_N) = \frac{1}{Z_N} \prod_{1 \leq i < j \leq N} (\lambda_i - \lambda_j)^2 \prod_{i=1}^N e^{-\lambda_i^2/2N}. \quad (9)$$

The above-mentioned semicircle law can be derived from this expression. Beyond the average eigenvalue density, one is also interested in finer statistical properties, such as the distribution of the largest eigenvalue  $\lambda_{\max}$ . This is computed by integrating the joint probability desnity as follows:

$$\text{Prob}(\lambda_{\max} \leq s) = \int_{(-\infty, s]^N} p(\lambda_1, \dots, \lambda_N) d\lambda_1 \cdots d\lambda_N. \quad (10)$$

By a large  $N$  asymptotic analysis one arrives at the GUE Tracy-Widom distribution<sup>23</sup> argued in the text.

A similar analysis can be performed for the Gaussian orthogonal ensemble (GOE), which is a counterpart of GUE for real symmetric matrices. The main difference is that in the expression for the joint probability distribution of eigenvalues the power of the Vandermonde determinant  $\prod_{1 \leq i < j \leq N} (\lambda_i - \lambda_j)$  is reduced from two to one. In the application of random matrices to quantum mechanics, this corresponds to Hamiltonian with no external magnetic field and thus to time reversal

symmetry. The change of the power leads to a different limiting distribution for the largest eigenvalue, namely the GOE Tracy-Widom distribution<sup>24</sup>.

These distributions have a strong universality. In a wide class of random matrix ensembles with and without time reversal symmetry, the Vandermonde determinant appears in their joint eigenvalue distribution with the power of one and two, respectively. The Gaussian factor in equation (9) may then be replaced by other weights, but the difference does not play an important role in the asymptotics and the largest eigenvalue is still described by the corresponding Tracy-Widom distribution.

## 2.2. Connection to growth models, curved vs. flat initial profile

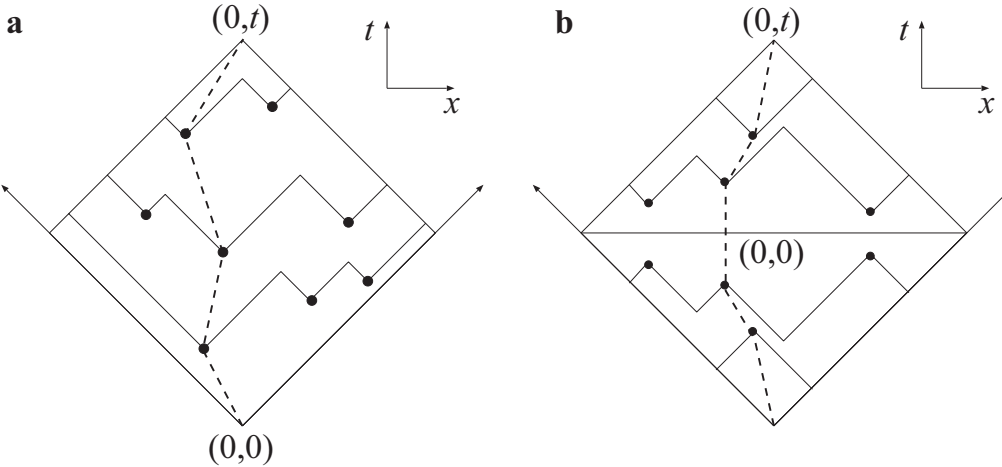
The connection between growth models and random matrix theory is best explained by using a simple example, for which we consider a model called the polynuclear growth (PNG) model. Suppose, at time  $t = 0$ , there is a nucleation event at the origin  $x = 0$  with unit height on a flat substrate (Supplementary Fig. 5). It grows in both horizontal directions with unit speed and forms the ground layer. On this ground layer random nucleations occur uniformly at a constant rate. Each up step, which we call a kink, moves to the left and each anti-kink, a down step, to the right with speed one. When a kink meets an anti-kink, they annihilate each other, *i.e.*, the two layers merge to one. Supplementary Fig. 5 shows an example of this growth at  $t = 0, 1, 2, 3, 4$  when nucleations occur at  $(x, t) = (-0.8, 1.6), (1.4, 2.6), (2.6, 3), (-0.4, 3.6)$ .

To analyse the height distribution of the PNG model, it is useful to draw a space-time diagram as in Supplementary Fig. 6a. Nucleation events are indicated by black dots and the trajectories of the (anti-)kinks are represented by the solid line segments. We then consider a directed path from the origin  $(0, 0)$  to  $(x = 0, t)$  such that the time  $t$  can only increase and the displacement in  $x$  is always smaller than the time increment. Such a path is represented by a set of points  $\{(x_i, t_i), 0 \leq i \leq m\}$  with  $(x_0, t_0) = (0, 0)$ ,  $(x_m, t_m) = (0, t)$  and  $|x_i - x_{i-1}| < t_i - t_{i-1}$ . The height  $h(0, t)$  of the PNG model is then given simply by the maximum number of nucleation events that such a directed path can go through. Analysis of the stochastic evolution is thereby translated into an optimisation problem.

Mathematically, this optimisation can be dealt with as a combinatorial problem, which then leads to the following expression for the height cumulative distribution:

$$\text{Prob}[h(0, t) \leq k] = \sum_{n=0}^{\infty} \sum_{\Lambda: |\Lambda|=n, \Lambda_1 \leq k} (f^\Lambda)^2 \frac{t^{2n} e^{-t^2}}{(n!)^2}. \quad (11)$$

Here,  $\Lambda$  denotes a Young diagram, which is an array of boxes arranged so that each row has the same or smaller number of boxes than the preceding one, as shown in Supplementary Fig. 7. The size of the Young diagram,  $|\Lambda|$ , is given by the total number of boxes. Now we fill each box of a Young diagram  $\Lambda$  with a number from  $\{1, 2, \dots, |\Lambda|\}$ , on condition that in each row and column the numbers are increasing rightward and downward. This is called the Standard Young tableau (SYT). The quantity  $f^\Lambda$  in the right-hand side of equation (11) is then the number of possible SYTs for a



**Supplementary Figure 6** | Space-time diagram for the PNG model in the droplet (a) and the flat (b) case. The dotted line is an optimal directed path.

$$\Lambda = \begin{array}{|c|c|c|}\hline & & \\ \hline \end{array}, \quad T = \begin{array}{|c|c|c|c|}\hline 1 & 2 & 4 & 9 \\ \hline 3 & 5 & 7 & \\ \hline 6 & & & \\ \hline 8 & & & \\ \hline \end{array}$$

**Supplementary Figure 7** | A Young diagram  $\Lambda$  and a standard Young tableau  $T$

given Young diagram  $\Lambda$ . It is known that  $f^\Lambda$  can be written as a Vandermonde determinant. It is squared in equation (11), and in this respect it is similar to equation (10) with (9). A main difference is the extra summation over  $n$  in equation (11), but it turns out that when  $t$  is large the summands with  $n \approx t$  have dominant contribution and the asymptotic analysis leads to the GUE Tracy-Widom distribution as defined in equation (10)<sup>31,38</sup>. This fact was first shown by Baik, Deift, Johansson in the context of statistics of longest increasing subsequence in random permutations<sup>38</sup>. This revealed the unexpected link between random matrix theory and combinatorics and then has led to the deep understanding of surface growth phenomena.

Along the same lines one can also study the flat interfaces of the PNG model. In this case one starts again from a flat substrate, but now nucleations occur everywhere, and hence there is no distinguished ground layer. In the space-time representation, this amounts to considering a triangle indicated in Supplementary Fig. 6b above the substrate  $t = 0$ . Now the height  $h(0, t)$  is given by the maximum number of nucleation points along a directed path, which starts here from any point on the base of the triangle. It is equal to half the number of points passed by the directed path inside the rectangle shown in Supplementary Fig. 6b, which is defined with a mirror image with respect to the  $x$ -axis. This then results in the same optimisation problem as for the curved PNG interfaces, except that now we have an additional time reversal symmetry for the nucleation events.

The combinatorics of SYTs are then rendered, and correspondingly the power of  $f^\Lambda$  in the height distribution formula changes from two to one. This finally yields the GOE Tracy-Widom distribution for the height distribution function, as for the case of GOE in random matrix theory.

All of these rather mathematical arguments do not hold, of course, for generic growth processes including the experimental system we have studied. Nevertheless, the resulting statistics for the height distribution has turned out to be robust, arising universally in the growth processes in the KPZ class, as demonstrated by our experiment.

## Supplementary Movie Legends

Movie S1: Growing DSM2 cluster with a circular interface. The movie shows a region of size  $3.03 \times 2.27 \text{ mm}^2$  and is played at five times real-time.

Movie S2: Growing DSM2 cluster with a flat interface. The movie shows a region of size  $3.03 \times 2.27 \text{ mm}^2$  and is played at five times real-time.

## Supplementary References

- [35] Wigner, E. P. On the statistical distribution of the widths and spacings of nuclear resonance levels. *Math. Proc. Cambridge Philos. Soc.* **47**, 790-798 (1951).
- [36] Forrester, P. J. *Log-Gases and Random Matrices* (Princeton Univ. Press, Princeton, Oxford, 2010).
- [37] Akemann, G., Baik, J. & Di Fransesco, P. (eds) *The Oxford Handbook on Random Matrix Theory* (Oxford Univ. Press, Oxford, 2010).
- [38] Baik, J., Deift, P. A. & Johansson, K. On the distribution of the length of the longest increasing subsequence of random permutations. *J. Amer. Math. Soc.* **12**, 1119-1178 (1999).